9644 *Inorg. Chem.* **2009**, *48*, 9644–9652
DOI: 10.1021/ic9007137

Inorganic Chemistry
Article

Systematic Manipulation of the Light-Harvesting Properties for Tridentate Cyclometalated Ruthenium(II) Complexes

Bryan D. Koivisto, Kiyoshi C. D. Robson, and Curtis P. Berlinguette*

Department of Chemistry and The Institute of Sustainable Energy, Environment and Economy, University of Calgary, 2500 University Drive N.W., Calgary, Canada T2N-1N4

Received April 11, 2009

The response of the metal-to-ligand charge-transfer (MLCT) band to variability in terminal substituents within a related set of tridentate polypyridyl and cyclometalated Ru(II) complexes is reported. These complexes are formulated as $[Ru(tpy\text{-}R^1)(tpy\text{-}R^2)](PF_6)_2$ (**1**−**6**; tpy=2,2′:6′,2″-terpyridine; R^1=−H, −2-furyl, or −OMe; R^2=−H, −2-furyl, or $-CO_2H$) and $[Ru(tpy\text{-}R^2)(dpb\text{-}R^1)]PF_6$ (**7**−**10**; Hdpb=1,3-di(pyridin-2-yl)benzene; R^2=−H or −2-furyl; R^1=−H or −OMe). Absorption spectra for the $[Ru(tpy\text{-}R^1)(tpy\text{-}R^2)]^{2+}$ series highlight the sensitivity of the MLCT band to the indicated substituents at the 4′ position of one or both tpy ligands (e.g., a bathochromic shift up to 24 nm coupled with a 2-fold increase in absorption intensity). Similar observations are made for the $[Ru(tpy\text{-}R^2)(dpb\text{-}R^1)]^+$ series, where a single Ru−N dative bond is replaced by a Ru−C σ-bond to form a cyclometalated complex. The reduced symmetry at the metal center within this series results in a broadening of the lowest-energy MLCT band, while an additional set of transitions at higher energies emerges that involves an excited state localized on the cyclometalating ligand. These MLCT transitions collectively render a broad absorption envelope of substantial intensity at wavelengths longer than ca. 525 nm. Optimal results are obtained for compound **10** (R^1=−OMe; R^2=−2-furyl), where a strong electron-donating group is situated para to the Ru−C bond (λ_{max}=523 nm; ε=2.6 × 10^4 M^{-1} cm^{-1}). This approach imparts substantial polarization within the molecule, which should benefit excited-state electron-transfer reactions for photosensitizing applications (e.g., dye-sensitized solar cells). Spectroscopic data are corroborated by electrochemical and TD-DFT measurements for all compounds.

Introduction

A mononuclear cyclometalated Ru(II) chromophore was recently shown to exhibit an overall conversion efficiency of 10.1% in the dye-sensitized solar cell (DSSC).[1] This finding is an important advancement because the complex, $[Ru(dcbpy)_2(ppy\text{-}F_2)]^+$ (dcbpy = bis(4,4′-dicarboxy-2,2′-bipyridine; ppy-F_2= 2-(2,4-difluorophenyl)pyridine), is the most efficient dye reported to date that does not contain NCS^- ligands.[2,3] This design, which builds on a previous report by van Koten et al.,[4] provides an impetus to investigate this class of compounds in further detail.

The principles of operation for a prototypical Ru-based dye (e.g., $[Ru(dcbpy)_2(NCS)_2]$ (**N3**)) in the DSSC involve a photoinduced metal-to-ligand charge-transfer (MLCT) transition, followed by rapid charge injection into the semiconductor anode.[2,5] There is currently a strong push to develop dyes that harness a greater fraction of the solar spectrum by driving the MLCT band to longer wavelengths.[6] The common approach is to lower the ligand-based lowest unoccupied molecular orbital (LUMO), or to raise the energy of the metal-based highest occupied molecular orbital (HOMO) using strong electron-donating ligands (e.g., NCS^-).[2]

Following an alternative approach, we[7] and others[1,4] have set out to explore the viability of using cyclometalated Ru complexes[8,9] as dyes in the DSSC setting. Expanding on the work of Constable et al.[10−14] and others,[15−26] we confirmed

*To whom correspondence should be addressed. E-mail: cberling@ucalgary.ca.

(1) Bessho, T.; Yoneda, E.; Yum, J.-H.; Guglielmi, M.; Tavernelli, I.; Imai, H.; Rothlisberger, U.; Nazeeruddin, M. K.; Grätzel, M. *J. Am. Chem. Soc.* **2009**, *131*, 5930−5934.
(2) Grätzel, M. *Inorg. Chem.* **2005**, *44*, 6841–6851.
(3) Grätzel, M. *Nature* **2001**, *414*, 338–344.
(4) Wadman, S. H.; Kroon, J. M.; Bakker, K.; Lutz, M.; Spek, A. L.; van Klink, G. P. M.; van Koten, G. *Chem. Commun.* **2007**, 1907–1909.
(5) Ardo, S.; Meyer, G. J. *Chem. Soc. Rev.* **2009**, *38*, 115–164.
(6) Robertson, N. *Angew. Chem., Int. Ed.* **2008**, *47*, 1012–1014.
(7) Bomben, P. G.; Robson, K. C. D; Sedach, P. A.; Berlinguette, C. P. *Inorg. Chem.* **2009**, DOI: 10.1021/ic900653q.
(8) Bruce, M. I. *Angew. Chem.* **1977**, *89*, 75–89.
(9) Djukic, J. P.; Sortais, J. B.; Barloy, L.; Pfeffer, M. *Eur. J. Inorg. Chem.* **2009**, 817–853.
(10) Constable, E. C.; Hannon, M. J. *Inorg. Chim. Acta* **1993**, *211*, 101–10.
(11) Constable, E. C.; Thompson, A. M. W. C.; Tocher, D. A.; Daniels, M. A. M. *New J. Chem.* **1992**, *16*, 855–67.
(12) Constable, E. C.; Housecroft, C. E. *Polyhedron* **1990**, *9*, 1939–1947.
(13) Constable, E. C.; Leese, T. A. *J. Organomet. Chem.* **1987**, *335*, 293–299.
(14) Constable, E. C.; Holmes, J. M. *J. Organomet. Chem.* **1986**, *301*, 203–8.
(15) Barigelletti, F.; Ventura, B.; Collin, J.-P.; Kayhanian, R.; Gavina, P.; Sauvage, J.-P. *Eur. J. Inorg. Chem.* **2000**, 113–119.
(16) Patoux, C.; Launay, J.-P.; Beley, M.; Chodorowski-Kimmes, S.; Collin, J.-P.; James, S.; Sauvage, J.-P. *J. Am. Chem. Soc.* **1998**, *120*, 3717–3725.

 Published on Web 09/23/2009

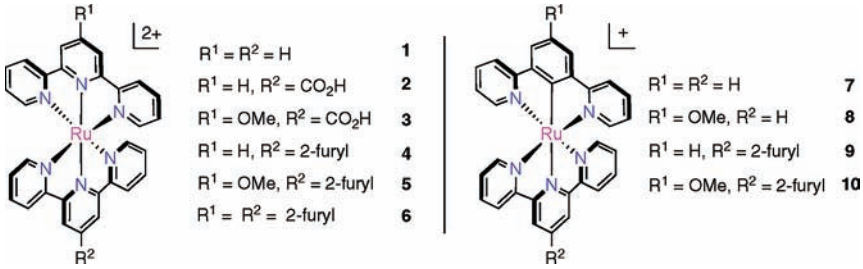

Figure 1. Schematic representations of Ru(II) complexes under investigation. (Counterion = PF_6^- for all complexes.)

that the substitution of a Ru−N dative bond with a Ru−C σ-bond is an effective strategy for shifting the absorbance profile closer to the near-infrared region.[7] In this study, we converge on a series of tridentate complexes structurally related to $[Ru(tpy)_2]^{2+}$ (tpy = 2,2′:6′,2″-terpyridine). Aligned with a recent study by van Koten et al. that catalogs the properties of a related series of complexes,[27] we set out to manipulate the electronic structure of molecules of the type $[Ru(tpy)(N^\wedge C^\wedge N)]^+$, with the overarching goal of increasing the molar extinction coefficient (ε) while inducing a bathochromic shift in the absorption profile.

Cognizant that there is significant contribution from the cyclometalating ligand to the HOMO,[26,27] we targeted a series of molecules with electron-donating substituents at the para position of the cyclometalating ligand and electron-withdrawing groups at the 4′ position of tpy to shift the MLCT bands to longer wavelengths. Herein, we report the thermodynamic and spectroscopic properties of a series of benchmark polypyridyl-based compounds $[Ru(tpy\text{-}R^1)(tpy\text{-}R^2)](PF_6)_2$ (**1**−**6**; R^1 = −H, −2-furyl, or −OMe; R^2 = −H, −2-furyl, or $-CO_2H$) and the cyclometalated congeners $[Ru(tpy\text{-}R^2)(dpb\text{-}R^1)]PF_6$ (**7**−**10**; Hdpb = 1,3-di(pyridin-2-yl)benzene; R^2 = −H or −2-furyl; R^1 = −H or −OMe) (Figure 1). Although a similar systematic approach has been carried out on polypyridyl[28,29] and, to a far lesser extent, cyclometalated compounds,[27] this study introduces a stronger electron-donating group (e.g., methoxy) to enhance the polarizabilty of the compound. This work shows that the MLCT bands that are relevant to light-harvesting applications can be manipulated in a predictable and systematic way by using these peripheral substituents.

Experimental Section

Preparation of Compounds. All reactions and manipulations were performed using solvents passed through an MBraun solvent purification system prior to use; chloroform ($CHCl_3$) and tetrahydrofuran (THF) solvents were analytical-grade (without a stabilizer). Unless stated otherwise, all reagents were purchased from Aldrich and used without further purification; $RuCl_3 \cdot 3H_2O$ was purchased from Pressure Chemical Company. Purification by column chromatography was carried out using silica (Silicycle: Ultrapure Flash Silica) or basic alumina (Fluka). Analytical thin-layer chromatography was performed on aluminum-backed sheets precoated with silica 60 F254 adsorbent (0.25 mm thick; Merck, Germany) or with plastic-backed sheets precoated with basic alumina 200 F254 adsorbent (0.25-mm-thick, Selecto Scientific: Suwanee, Georgia) and visualized under UV light. Routine ^1H and ^{13}C NMR spectra were recorded at 400 and 100 MHz, respectively, on a Bruker AV 400 instrument at ambient temperature unless otherwise stated. Chemical shifts (δ) are reported in parts per million from low to high field and referenced to residual nondeuterated solvent. Standard abbreviations indicating multiplicity are used as follows: d = doublet, m = multiplet, s = singlet, and t = triplet. All proton assignments correspond to the generic molecular scheme depicted in Figure 2. Elemental analysis, electrospray ionization (ESI), and high-resolution electron impact (EI) mass spectrometry (MS) data were collected at the University of Calgary. Ligands 4′-(furan-2-yl)-2,2′:6′,2″-terpyridine (**L2**),[30,31] 4′-methoxy-2,2′:6′,2″-terpyridine (**L3**),[32] and 1,3-di(pyridin-2-yl)benzene (**L5**)[33] and complexes $RuCl_3$(**L1**),[34] **1**,[28] **6**,[30] and **7**[27] were prepared according to published procedures (with additional purification steps using column chromotagraphy where necessary).

[$RuCl_3$(tpy-2-furyl)], $RuCl_3$(L2). A solution of tpy-2-furyl (286 mg, 0.956 mmol) and $RuCl_3 \cdot 3H_2O$ (250 mg, 0.956 mmol) in absolute EtOH (750 mL) was heated at reflux for 3 h. The solid was isolated by filtration and washed with EtOH (2 × 20 mL) and diethyl ether and dried to yield 400 mg of a red/brown solid product (yield = 82.6%). Anal. Calcd for

(17) Collin, J.-P.; Kayhanian, R.; Sauvage, J.-P.; Calogero, G.; Barigelletti, F.; De Cian, A.; Fischer, J. *Chem. Commun.* **1997**, 775–776.
(18) Collin, J. P.; Beley, M.; Sauvage, J. P.; Barigelletti, F. *Inorg. Chim. Acta* **1991**, *186*, 91–3.
(19) Ott, S.; Borgström, M.; Hammarström, L.; Johansson, O. *Dalton Trans.* **2006**, 1434–1443.
(20) Le Lagadec, R.; Rubio, L.; Alexandrova, L.; Toscano, R. A.; Ivanova, E. V.; Meskys, R.; Laurinavicius, V.; Pfeffer, M.; Ryabov, A. D. *J. Organomet. Chem.* **2004**, *689*, 4820–4832.
(21) Sortais, J.-B.; Pannetier, N.; Holuigue, A.; Barloy, L.; Sirlin, C.; Pfeffer, M.; Kyritsakas, N. *Organometallics* **2007**, *26*, 1856–1867.
(22) Leyva, L.; Sirlin, C.; Rubio, L.; Franco, C.; Le Lagadec, R.; Spencer, J.; Bischoff, P.; Gaiddon, C.; Loeffler, J. P.; Pfeffer, M. *Eur. J. Inorg. Chem.* **2007**, *2007*, 3055–3066.
(23) Saavedra-Diaz, O.; Ceron-Camacho, R.; Hernandez, S.; Ryabov, A. D.; Le Lagadec, R. *Eur. J. Inorg. Chem.* **2008**, 4866–4869.
(24) Ryabov, A. D.; Estevez, H.; Alexandrova, L.; Pfeffer, M.; Le Lagadec, R. *Inorg. Chim. Acta* **2006**, *359*, 883–887.
(25) Le Lagadec, R.; Alexandrova, L.; Estevez, H.; Pfeffer, M.; Laurinavicius, V.; Razumiene, J.; Ryabov, A. D. *Eur. J. Inorg. Chem.* **2006**, *2006*, 2735–2738.
(26) Alpeeva, I. S.; Soukharev, V. S.; Alexandrova, L.; Shilova, N. V.; Bovin, N. V.; Csoeregi, E.; Ryabov, A. D.; Sakharov, I. Y. *J. Biol. Inorg. Chem.* **2003**, *8*, 683–688.
(27) Wadman, S. H.; Lutz, M.; Tooke, D. M.; Spek, A. L.; Hartl, F.; Havenith, R. W. A.; van Klink, G. P. M.; van Koten, G. *Inorg. Chem.* **2009**, *48*, 1887–1900.
(28) Maestri, M.; Armaroli, N.; Balzani, V.; Constable, E. C.; Thompson, A. M. W. C. *Inorg. Chem.* **1995**, *34*, 2759–67.
(29) Juris, A.; Balzani, V.; Barigelletti, F.; Campagna, S.; Belser, P.; Von Zelewsky, A. *Coord. Chem. Rev.* **1988**, *84*, 85–277.
(30) Constable, E. C.; Dunphy, E. L.; Housecroft, C. E.; Neuburger, M.; Schaffner, S.; Schaper, F.; Batten, S. R. *Dalton Trans.* **2007**, 4323–4332.
(31) Husson, J.; Beley, M.; Kirsch, G. *Tetrahedron Lett.* **2003**, *44*, 1767–1770.
(32) Chambers, J.; Eaves, B.; Parker, D.; Claxton, R.; Ray, P. S.; Slattery, S. J. *Inorg. Chim. Acta* **2006**, *359*, 2400–2406.
(33) Soro, B.; Stoccoro, S.; Minghetti, G.; Zucca, A.; Cinellu, M. A.; Gladiali, S.; Manassero, M.; Sansoni, M. *Organometallics* **2005**, *24*, 53–61.
(34) Sullivan, B. P.; Calvert, J. M.; Meyer, T. J. *Inorg. Chem.* **1980**, *19*, 1404–7.

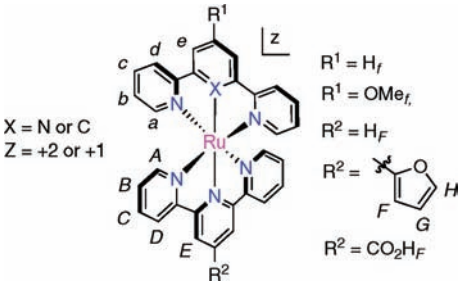

Figure 2. Labeling scheme for the assignment of ^{1}H NMR signals.

$C_{19}H_{13}Cl_3N_3ORu$: C, 45.03; H, 2.59; N, 8.29. Found: C, 44.94; H, 2.78; N, 8.14.

2,2′-(5-Methoxy-1,3-phenylene)dipyridine (Hdpb-OMe; L4). A THF (150 mL) solution containing 1,3-dibromo-5-methoxybenzene (1.10 g, 4.10 mmol) and $Pd(PPh_3)_4$ (0.48 g, 0.41 mmol) was charged with a 0.5 M THF solution of 2-pyridylzinc bromide (21 mL, 10 mmol). The solution was stirred at reflux for 14 h, cooled, and then quenched with a saturated aqueous $NaHCO_3$ solution (100 mL) and washed with aqueous EDTA. The crude product was extracted with diethyl ether (2 × 100 mL), and the organic fractions were collected and dried over $MgSO_4$. The solvent was removed in vacuo to afford an oil that was purified by column chromatography [Al_2O_3: Et_2O, R_f = 0.60]; the resultant oily product converted to a white solid upon standing (850 mg; yield = 78%). ^{1}H NMR (300 MHz, $CDCl_3$): δ 8.70 (d, 2H, ^3J = 7 Hz, H_d), 8.20 (s, 1H, H_f), 7.77 (d, 2H, ^3J = 8 Hz, H_a), 7.75 (t, 2H, ^3J = 8 Hz, H_b), 7.66 (s, 2H, H_e), 7.25 (t, 2H, ^3J = 8 Hz, H_c), 3.97 (s, 3H, H_g). ^{13}C NMR (100 MHz, $CDCl_3$): δ 160.7, 157.2, 149.7, 141.4, 136.9, 122.5, 121.0, 118.2, 113.3, 55.8. HRMS (EI): m/z 262.1101 [$(M)^+$] (calcd for $C_{17}H_{14}N_2O^+$: m/z 262.1106).

[Ru(tpy)(tpy-CO$_2$H)](PF$_6$)$_2$ (2). Solid $KMnO_4$ (1.94 g, 30 equiv) was added to [Ru(tpy)(tpy-2-furyl)]$(NO_3)_2$ (310 mg, 0.41 mmol) in 30 mL of H_2O and then stirred at room temperature overnight. After the mixture was filtered to remove MnO_2, solvent was removed, and the solid was then preabsorbed on silica. The target complex was isolated as the orange band from column chromatography [SiO_2: acetone/MeOH/sat. aq. KNO_3, 6:3:1]. The resultant solid was reconstituted in water and acidified using acetic acid, and the product precipitated as the PF_6^- salt using saturated aqueous NH_4PF_6 to yield 230 mg of a red solid product (yield = 62%). ^{1}H NMR (400 MHz, CD_3CN): δ 9.34 (s, 2H, H_E), 8.77 (d, 2H, ^3J = 8 Hz, H_e), 8.68 (d, 2H, ^3J = 8 Hz, H_D), 8.50 (d, 2H, ^3J = 8 Hz, H_d), 8.43 (t, 1H, ^3J = 8 Hz, H_f), 7.93 (ddd, 4H, ^3J = 8 Hz, 7 Hz, ^4J = 1 Hz, H_C, H_c), 7.40 (d, 2H, ^3J = 7 Hz, H_A), 7.36 (d, 2H, ^3J = 7 Hz, H_a), 7.18 (ddd, 2H, ^3J = 8 Hz, 7 Hz, ^4J = 1 Hz, H_B), 7.16 (ddd, 2H, ^3J = 8 Hz, 7 Hz, ^4J = 1 Hz, H_b). ESI-MS: m/z 567.15 [$(M-CO_2H-2PF_6)^+$] (calcd for $C_{30}H_{22}N_6Ru^+$: m/z 567.09). Anal. Calcd for $C_{31}H_{22}F_{12}N_6O_2P_2Ru\cdot H_2O$: C, 40.49; H, 2.63; N, 9.14. Found: C, 40.58; H, 2.78; N, 8.73.

[Ru(tpy-OMe)(tpy-CO$_2$H)](PF$_6$)$_2$ (3). Solid $KMnO_4$ (963 mg, 30 equiv) was added to [Ru(tpy-OMe)(tpy-2-furyl)]$(NO_3)_2$ (160 mg, 0.20 mmol) in 30 mL of water and stirred at room temperature for 12 h. The solvent was removed after filtration, and the solid was then preabsorbed on silica. The target complex was collected as an orange band using column chromatography [SiO_2: acetone/MeOH/sat. aq. KNO_3, 6:3:1]. Following the removal of the solvent, the solid was reconstituted in water and acidified using acetic acid, and the product precipitated as the PF_6^- salt using saturated aqueous NH_4PF_6 to yield 130 mg of the red product (yield = 68%). ^{1}H NMR (400 MHz, CD_3OD): δ 9.24 (s, 2H, H_E), 8.65 (d, 2H, ^3J = 8 Hz, H_D), 8.62 (d, 2H, ^3J = 8 Hz, H_d), 8.51 (s, 2H, H_e), 7.98 (ddd, 2H, ^3J = 8 Hz, 7 Hz, ^4J = 1 Hz, H_C), 7.94 (ddd, 2H, ^3J = 8 Hz, 7 Hz, ^4J = 1 Hz, H_c), 7.49 (d, 2H, ^3J = 7 Hz, H_A), 7.38 (d, 2H, ^3J = 7 Hz, H_a), 7.24 (ddd, 2H, ^3J = 8 Hz, 7 Hz, ^4J = 1 Hz, H_B), 7.17 (ddd, 2H, ^3J = 8 Hz, 7 Hz, ^4J = 1 Hz, H_b), 4.36 (s, 3H, H_f). ESI-MS: m/z 597.12 [$(M-CO_2H-2PF_6)^+$] (calcd for $C_{31}H_{23}N_6ORu^+$: m/z 597.10). Anal. Calcd for $C_{32}H_{24}F_{12}N_6O_3P_2Ru$: C, 41.26; H, 2.66; N, 9.02. Found: C, 41.41; H, 3.16; N, 8.88.

General Synthetic Procedure for Complexes 4−10. A flask containing 0.40 mmol of $RuCl_3$(**L1** or **L2**) and 0.40 mmol of **L1**, **L2**, **L3**, **L4**, or **L5** in 30 mL of a MeOH/H_2O (5:1 v/v) mixed solvent system and five drops of *N*-ethylmorpholine was stirred at reflux under N_2 for 10 h. The solvent was then removed in vacuo, and the crude mixture was preabsorbed onto either silica or basic alumina (conditions provided below).

[Ru(tpy)(tpy-2-furyl)](PF$_6$)$_2$ (4). Compound **4** was collected as a red band using column chromatography [SiO_2/acetone/MeOH/sat. aq. KNO_3, 5:2:1]. The solvent was removed and the product precipitated as the PF_6^- salt using saturated aqueous NH_4PF_6 to yield 230 mg of the red product (yield = 61%). ^{1}H NMR (400 MHz, CD_3CN): δ 8.97 (s, 2H, H_E), 8.76 (d, 2H, ^3J = 8 Hz, H_D), 8.62 (d, 2H, ^3J = 8 Hz, H_d), 8.50 (d, 2H, ^3J = 8 Hz, H_e), 8.41 (t, 1H, ^3J = 8 Hz, H_f), 7.97−7.87 (m, 5H, H_C, H_c, H_H), 7.62 (d, 1H, ^3J = 4 Hz, H_F), 7.43 (d, 2H, ^3J = 7 Hz, H_A), 7.34 (d, 2H, ^3J = 7 Hz, H_a), 7.16 (m, 4H, H_B, H_b), 6.87 (dd, 1H, ^3J = 4 Hz, 2 Hz, H_G). ESI-MS: m/z 778.94 [$(M-PF_6)^+$] (anal. calcd for $C_{34}H_{24}F_6N_6OPRu^+$: m/z 779.07). Anal. Calcd for $C_{34}H_{24}F_{12}N_6OP_2Ru\cdot H_2O$: C, 43.37; H, 2.78; N, 8.93. Found: C, 43.29; H, 2.90; N, 8.54.

[Ru(tpy-OMe)(tpy-2-furyl)](PF$_6$)$_2$ (5). Compound **5** was collected as a red band using column chromatography [SiO_2: acetone/MeOH/sat. aq. KNO_3, 5:2:1]. The solvent was removed and the product precipitated as the PF_6^- salt using saturated aqueous NH_4PF_6 to yield 250 mg of the red product (yield = 65%). ^{1}H NMR (400 MHz, CD_3CN): δ 8.95 (s, 2H, H_E), 8.61 (d, 2H, ^3J = 8 Hz, H_D), 8.49 (d, 2H, ^3J = 8 Hz, H_d), 8.33 (s, 2H, H_e), 7.97−7.86 (m, 5H, H_C, H_c, H_H), 7.60 (d, 1H, ^3J = 4 Hz, H_F), 7.42 (d, 2H, ^3J = 7 Hz, H_A), 7.38 (d, 2H, ^3J = 7 Hz, H_a), 7.19 (ddd, 2H, ^3J = 8 Hz, 7 Hz, ^4J = 1 Hz, H_B), 7.12 (ddd, 2H, ^3J = 8 Hz, 7 Hz, ^4J = 1 Hz, H_b), 6.86 (dd, 1H, ^3J = 4 Hz, 2 Hz, H_G), 4.31 (s, 3H, H_f). ESI-MS: m/z 809.05 [$(M-PF_6)^+$] (calcd for $C_{35}H_{26}F_6N_6O_2PRu^+$: m/z 809.08). Anal. Calcd for $C_{35}H_{26}F_{12}N_6O_2P_2Ru$: C, 44.08; H, 2.75; N, 8.81. Found: C, 44.37; H, 3.05; N, 9.02.

[Ru(dpb-OMe)(tpy)]PF$_6$ (8). Compound **8** was collected as the first purple band via column chromatography [SiO_2: acetone/MeOH/sat. aq. KNO_3, 2:1:1]. The solvent was removed and the product precipitated as the PF_6^- salt using saturated aqueous NH_4PF_6 to yield 120 mg of a deep red/purple product (yield = 40%). ^{1}H NMR (400 MHz, CD_3OD): δ 8.87 (d, 2H, H_E), 8.54 (d, 2H, ^3J = 8 Hz, H_D), 8.26 (t, 1H, ^3J = 8 Hz, H_F), 8.17 (d, 2H, ^3J = 8 Hz, H_d), 8.00 (s, 2H, H_e), 7.71 (ddd, 2H, ^3J = 8 Hz, 7 Hz, ^4J = 1 Hz, H_C), 7.61 (ddd, 2H, ^3J = 8 Hz, 7 Hz, ^4J = 1 Hz, H_c), 7.17 (d, 2H, ^3J = 7 Hz, H_A), 6.99 (ddd, 2H, ^3J = 8 Hz, 7 Hz, ^4J = 1 Hz, H_B), 6.97 (d, 2H, ^3J = 7 Hz, H_a), 6.66 (ddd, 2H, ^3J = 8 Hz, 7 Hz, ^4J = 1 Hz, H_b), 4.00 (s, 3H, H_f). ESI-MS: m/z 596.18 [$(M-PF_6)^+$] (anal. calcd for $C_{32}H_{24}N_5ORu^+$: m/z 596.10). Anal. Calcd for $C_{32}H_{24}F_6N_5OPRu\cdot 2H_2O$: C, 49.49; H, 3.63; N, 9.02. Found: C, 49.29; H, 3.33; N, 8.73.

[Ru(dpb)(tpy-2-furyl)]PF$_6$ (9). Compound **9** was collected as a purple band using column chromatography [basic Al_2O_3: acetone saturated with KPF_6 and ascorbic acid]. After removal of the solvent, the product suspended in water, filtered, and then washed with Et_2O to yield 170 mg of a red product (yield = 53%). ^{1}H NMR (400 MHz, CD_3CN): δ 8.98 (s, 2H, H_E), 8.54 (d, 2H, ^3J = 8 Hz, H_D), 8.25 (d, 2H, ^3J = 8 Hz, H_e), 8.13 (d, 2H, ^3J = 8 Hz, H_d), 7.90 (d, 1H, ^3J = 2 Hz, H_H), 7.70 (ddd, 2H, ^3J = 8 Hz, 7 Hz, ^4J = 1 Hz, H_C), 7.58 (ddd, 2H, ^3J = 8 Hz, 7 Hz, ^4J = 1 Hz, H_c), 7.52 (d, 1H, ^3J = 4 Hz, H_F), 7.46 (t, 1H, ^3J = 8 Hz, H_f), 7.11 (d, 2H, ^3J = 7 Hz, H_A), 7.09 (d, 2H, ^3J = 7 Hz, H_a), 6.94 (ddd, 2H, ^3J = 8 Hz, 7 Hz, ^4J = 1 Hz, H_B), 6.83 (dd, 1H, ^3J = 4 Hz, 2 Hz, H_G), 6.64 (ddd, 2H, ^3J = 8 Hz, 7 Hz, ^4J = 1 Hz, H_b). ESI-MS: m/z 632.14

$[(M-PF_6)^+]$ (anal. calcd for $C_{35}H_{24}N_5ORu^+$: *m*/*z* 632.10). Anal. Calcd for $C_{35}H_{24}F_6N_5OPRu \cdot 2H_2O$: C, 51.73; H, 3.47; N, 8.62. Found: C, 51.30; H, 3.27; N, 8.93.

[Ru(dpb-OMe)(tpy-2-furyl)]PF_6 (10). Compound **10** was collected as a purple band using column chromatography [basic Al_2O_3: acetone saturated with KPF_6 and ascorbic acid]. The solvent was removed, suspended in water, then filtered and washed with Et_2O to yield 190 mg of a purple solid (57%). ^{1}H NMR (400 MHz, CD_3CN): δ 8.98 (s, 2H, H_E), 8.53 (d, 2H, ^3J=8 Hz, H_D), 8.13 (d, 2H, ^3J=8 Hz, H_d), 7.97 (s, 2H, H_e), 7.90 (d, 1H, ^3J=2 Hz, H_H), 7.70 (ddd, 2H, ^3J=8 Hz, 7 Hz, ^4J=1 Hz, H_C), 7.57 (ddd, 2H, ^3J=8 Hz, 7 Hz, ^4J=1 Hz, H_c), 7.52 (d, 1H, ^3J=4 Hz, H_F), 7.13 (d, 2H, ^3J=7 Hz, H_A), 7.07 (d, 2H, ^3J=7 Hz, H_a), 6.96 (ddd, 2H, ^3J=8 Hz, 7 Hz, ^4J=1 Hz, H_B), 6.82 (dd, 1H, ^3J=4 Hz, 2 Hz, H_G), 6.62 (ddd, 2H, ^3J=8 Hz, 7 Hz, ^4J=1 Hz, H_b), 4.32 (s, 3H, H_f). ESI-MS: *m*/*z* 662.18 $[(M-PF_6)^+]$ (anal. calcd for $C_{36}H_{26}N_5O_2Ru^+$: *m*/*z* 662.11). Anal. Calcd for $C_{36}H_{26}F_6N_5O_2PRu \cdot 2H_2O$: C, 51.31; H, 3.59; N, 8.31. Found: C, 50.83; H, 3.29; N, 8.11.

Physical Methods. Electrochemical measurements were performed under anaerobic conditions. Electrochemical measurements were made with a Princeton Applied Research VersaStat 3 potentiostat using dry solvents, a Pt working electrode, a Ag reference electrode, and a 0.1 M NBu_4BF_4 supporting electrolyte. Potentials were initially referenced to an internal ferrocene (Fc) standard; however, potentials reported herein are referenced to a normal hydrogen electrode (NHE) on the premise that the Fc/Fc^+ couple occurs at +0.640 V versus NHE in MeCN.[35] Electronic spectroscopic data were collected on MeCN solutions using a Cary 5000 UV−vis spectrophotometer (Varian).

DFT Calculations. Density functional theory calculations were carried out using B3LYP (Becke's three-parameter exchange functional (B3) and the Lee−Yang−Parr correlation functional (LYP)) and the LanL2DZ basis set. All geometries were fully optimized in the ground states (closed-shell singlet S_o). Time-dependent density functional theory (TD-DFT) calculations were performed with a spin-restricted formalism to examine low-energy excitations at the ground-state geometry (output files are provided as Supporting Information). All calculations were carried out with the Gaussian 03W software package.

Results

Synthesis and Characterization. Ru(II) complexes containing 4′-methoxy-substituted tridendate ligands have been previously synthesized,[36] but this ligand remains absent from studies of heteroleptic Ru complexes studying the effects of various donor and acceptor ligands in a systematic way.[11,28,37] The −OMe substituent is a reasonably good donor when considering the Hammett constant of −0.27;[32] thus, it was anticipated that this donor would be effective at raising the HOMO level of Ru complexes to induce a bathochromic shift in the absorption profile − a desirable feature in harnessing a greater fraction of incident solar radiation. It has also been shown that substitution of a neutral tridentate ligand with an anionic cyclometalating ligand is an effective way of inducing a bathochromic shift in the low-energy transitions for Ru(II) complexes.[7,27] Taking these factors into consideration, the physicochemical properties of a series of 4′-substituted cyclometalated and noncyclometalated Ru(II) complexes were investigated.

Scheme 1. Synthesis of the $[Ru(tpy\text{-}R^1)(tpy\text{-}R^2)](PF_6)_2$ (**1**−**6**) and $[Ru(tpy\text{-}R^2)(dpb\text{-}R^1)]PF_6$ (**7**−**10**) Series[a]

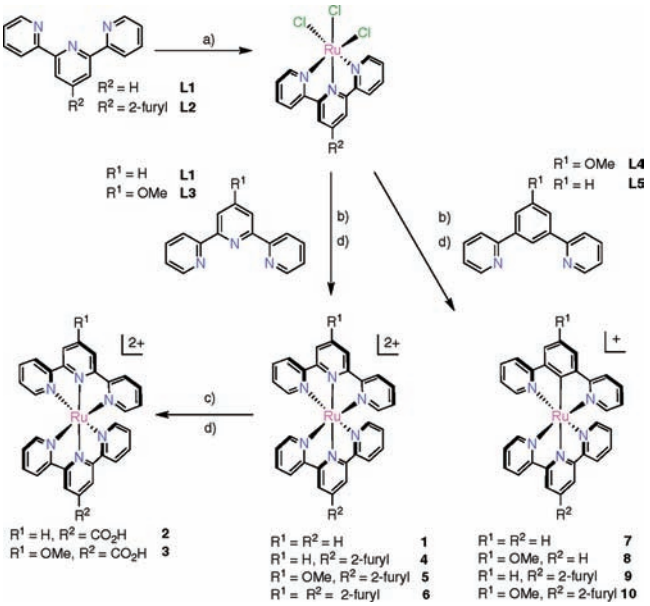

[a] Reaction conditions: (a) $RuCl_3$, EtOH, Δ, 12 h; (b) *N*-ethylmorpholine, Δ, 12 h; (c) $KMnO_4$, H_2O, RT, 16 h; (d) NH_4PF_6.

A typical procedure for the synthesis of heteroleptic terpyridyl and cyclometalated Ru complexes is presented in Scheme 1. Preparation of these heteroleptic complexes involves the initial coordination of a polypyridyl ligand to the Ru center (Scheme 1a), followed by the addition of the respective polypyridyl or cyclometalating ligand (Scheme 1b). Owing to the electronic demands of cyclometalation,[38] polypyridyl ligands were ligated first, followed by cyclometalation in the presence of a reductant (*N*-ethylmorpholine). Anion exchange reactions were carried out for all cationic complexes so that microcrystalline samples could be isolated; all analyses were carried out on the PF_6^- salts of the cationic complexes **1**−**10**. To advance our interests in the realm of sensitizing TiO_2 for solar cell applications, a 2-furyl group was used as a substituent because it has been shown to undergo oxidative cleavage to furnish a carboxylic acid anchoring group.[30] We could not, however, obtain the carboxylic acid products or recover our starting material when treating our cyclometalated complex with $KMnO_4$ − presumably a consequence of oxidative degradation of the complex (vide infra). Typical yields of the heteroleptic cyclometalated complexes are lower than those achieved with the analogous pyridyl-based reactions; this is likely a result of the additional purification steps (i.e., chromatography) required to separate the product from the common homoleptic byproducts (i.e., $[Ru(tpy\text{-}R)_2]^{2+}$). Furthermore, because of their electron-rich nature, some cyclometalated complexes require the addition of ascorbic acid to the eluent to prevent premature oxidation during the chromatography procedures.

(35) Pavlishchuk, V. V.; Addison, A. W. *Inorg. Chim. Acta* **2000**, *298*, 97–102.
(36) Dong, T. Y.; Lin, H. Y.; Lin, S. F.; Huang, C. C.; Wen, Y. S.; Lee L. S. *Organometallics* **2008**, *27*, 555–562.
(37) Balzani, V.; Juris, A.; Barigelletti, F.; Belser, P.; Von Zelewsky, A. *Sci. Pap. Inst. Phys. Chem. Res.* (*Jpn.*) **1984**, *78*, 78–85.
(38) Beley, M.; Collin, J. P.; Louis, R.; Metz, B.; Sauvage, J. P. *J. Am. Chem. Soc.* **1991**, *113*, 8521–8522.

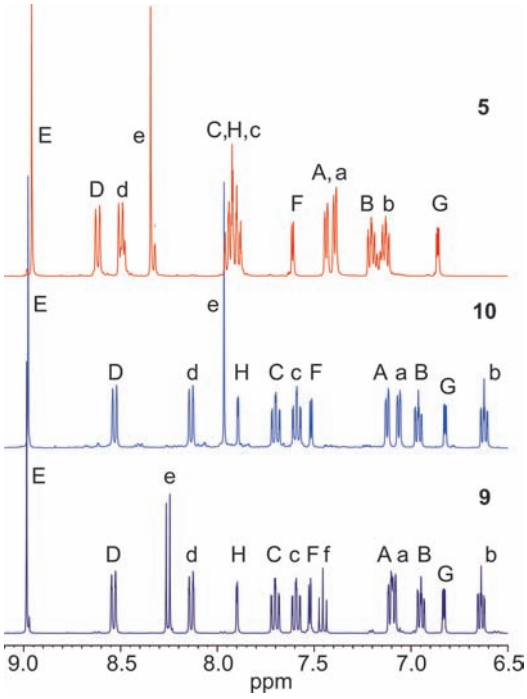

Figure 3. ^{1}H NMR spectra of compounds $[Ru(tpy\text{-}2\text{-}furyl)(tpy\text{-}OMe)]^{2+}$ (**5**), $[Ru(tpy\text{-}2\text{-}furyl)(dpb\text{-}OMe)]^{+}$ (**10**), and $[Ru(tpy\text{-}2\text{-}furyl)(dpb)]^{+}$ (**9**) in CD_3CN solutions at ambient temperature (only the aromatic region is shown). Signals are assigned according to the labeling scheme provided in Figure 2.

The identities of the complexes were verified by ESI-MS and ^{1}H NMR spectroscopy. ^{1}H NMR spectroscopy is a convenient tool for monitoring these reactions because cyclometalation results in a significant increase in electron density on the ligand.[7,10,14,27] The spectra provided in Figure 3 show the significance of cyclometalation and, to a lesser extent, the effects of −OMe substitution on the tpy ligand opposite the 2-furyl-substituted tpy (e.g., **5** and **10**). Upon cyclometalation, there are significant upfield shifts for all aromatic cyclometalating ligand proton signals. The polypyridyl ligand and the 2-furyl substituent protons (H_H, H_F, and H_G) experience modest upfield shifts consistent with increased electron density on the metal center and the π-accepting nature of the polypyridyl ligands. The addition of the −OMe substituent has a less dramatic effect on the chemical shift. There are strong upfield shifts on the phenyl ring protons (H_e) and small upfield perturbations in the adjacent pyridyl ring (H_d).

Electrochemical and Electronic Spectroscopic Behavior. The electrochemical and electronic absorption properties of **1**−**10** were examined in acetonitrile by cyclic voltammetry and UV−vis spectroscopy, respectively. Measured redox couples and absorption data for the terpyridine series **1**−**6** are reported in Table 1, and the cyclometalated series **7**−**10** is collected in Table 2. All compounds exhibit well-resolved redox couples over the +2 to −2 V (vs NHE) range.

The UV−vis absorption spectra for compounds **1**−**6** are provided in Figure 4; corresponding extinction coefficients and maxima corresponding to the lowest-energy excitation transitions are listed in Table 1. A common feature for the entire series is the presence of intense bands in the ultraviolet region between 250 and 350 nm (not shown), which are assigned as spin-allowed $^1(\pi-\pi^*)$ ligand transitions.[29] Examination of the lower-energy bands reveals systematic trends that are consistent with modest structural modifications. For instance, increasing the conjugation within the series results in a red shift of the λ_{max} with the concomitant increase in molar extinction coefficient. The first reversible oxidation process, which corresponds to a $Ru^{II/III}$ couple, is also sensitive to the nature of the tpy substituents. For example, the addition of a single −OMe group decreases the oxidation potential by approximately 70−80 mV, which is consistent with the value reported for 4′-ethoxy substitution.[28] Installation of the electron-rich, aromatic 2-furyl group decreases the oxidation potential by ca. 20 mV, while the electron-withdrawing $-CO_2H$ group increases the oxidation potential ca. 30 mV. The ligand-based reductions are also sensitive to ligand modification. The general trend that emerges from the series **1**−**6** is that extending the conjugation of the ligand shifts the LUMO to lower energy, while increasing electron density on the metal center raises the energy of the HOMO, and to a lesser extent the LUMO.

Electrochemical and spectroscopic data for **7**−**10** are listed in Table 2; data for compounds **11**−**14**, reported elsewhere,[19,27,39] are also provided for comparison. Representative cyclic voltammograms are also included in Figure 5. Unlike for the tpy series, there is only one observed reversible reduction wave within the solvent window for the cyclometalated analogues, which is assigned to the tpy ligand. Increasing conjugation on the tpy ligand results in a lower-energy ligand-based reduction process. The reversible oxidation wave is ascribed to a $Ru^{II/III}$ process and is significantly affected by cyclometalation. In contrast to the tpy series, the addition of the −OMe substituent to the cyclometalating ligand results in a substantial increase in electron density at the metal, causing a 130−140 mV decrease in the $Ru^{II/III}$ oxidation potential. Consistent with previous findings,[27] all of the cyclometalated complexes also have an irreversible oxidation at higher potentials (see Figure 5; data not tabulated) attributed to ligand-based decomposition. A ligand decomposition process is supported by the observation that the metal-based potential is sensitive to the presence of electron-donating groups, and as stated earlier, the cyclometalated 2-furyl-substituted complexes do not appear to survive oxidation by $KMnO_4$ in our hands.

The UV−vis absorption data with extinction coefficients and maxima corresponding to the lowest-energy absorption bands are listed in Table 2. An examination of the lower-energy bands reveals some significant differences relative to the tpy series. For instance, dissymmetry in the electronic structure of the heteroleptic cyclometalated complexes results in broadening of the spectral features (Figure 6), which is substantiated by the TD-DFT calculations (Figure 7). Complexes **5** and **10** exhibit similar molar extinction coefficients, but there is a significant broadening and a bathochromic shift for the spectrum corresponding to cyclometalated complex **10**, which is caused by the loss of degeneracy of the occupied

(39) Cazzanti, S.; Caramori, S.; Argazzi, R.; Elliott, C. M.; Bignozzi, C. A. *J. Am. Chem. Soc.* **2006**, *128*, 9996–9997.

Table 1. Summary of Select Electrochemical and Spectroscopic Data for Compounds **1**−**6**

	UV−vis data		redox data (V vs NHE)[a]		
compound	λ_{max}[b] (nm)	ε ($\times 10^4$ M^{-1} cm^{-1})	$E_{1/2}$ (ox)		$E_{1/2}$ (red)
$[Ru(tpy)_2](PF_6)_2$ (**1**)	476	1.54	1.52	−1.02	−1.27
$[Ru(tpy)(tpy\text{-}CO_2H)](PF_6)_2$ (**2**)	479	1.95	1.55	−1.05	−1.33
$[Ru(tpy\text{-}OMe)(tpy\text{-}CO_2H)](PF_6)_2$ (**3**)	484	1.94	1.48	−1.08	−1.32
$[Ru(tpy)(tpy\text{-}2\text{-}furyl)](PF_6)_2$ (**4**)	488	2.23	1.49	−0.93	−1.07
$[Ru(tpy\text{-}OMe)(tpy\text{-}2\text{-}furyl)](PF_6)_2$ (**5**)	495	2.50	1.41	−1.01	−1.26
$[Ru(tpy\text{-}2\text{-}furyl)_2](PF_6)_2$ (**6**)	500	3.19	1.48	−0.96	−1.20

[a] Data collected using 0.1 M NBu_4BF_4 MeCN solutions at 100 mV/s and referenced to a $[Fc]/[Fc]^+$ internal standard followed by conversion to NHE ($[Fc]/[Fc]^+$ vs NHE = +0.64 V).[35] [b] λ_{max} of lowest-energy band.

Table 2. Summary of Select Electrochemical and Spectroscopic Data for Compounds **7**−**14**

	UV−vis data		redox data (V vs NHE)[a]	
compound	λ_{max}[b] (nm)	ε ($\times 10^4$ M^{-1} cm^{-1})	$E_{1/2}$ (ox)	$E_{1/2}$ (red)
$[Ru(tpy)(dpb)]PF_6$ (**7**)	500	1.17	0.75	−1.32
$[Ru(tpy)(dpb\text{-}OMe)]PF_6$ (**8**)	535	1.59	0.62	−1.31
$[Ru(tpy\text{-}2\text{-}furyl)(dpb)]PF_6$ (**9**)	509	1.36	0.76	−1.26
$[Ru(tpy\text{-}2\text{-}furyl)(dpb\text{-}OMe)]PF_6$ (**10**)	523	2.59	0.62	−1.26
$[Ru(ttpy)(dpb)]PF_6$ (**11**[c])[19]	504	1.10	0.74	−1.35
$[Ru(ttpy)(dpb\text{-}phenyl)]PF_6$ (**12**[c])[19]	510	1.70	0.74	−1.24
$[Ru(tpy\text{-}CO_2Et)(dpb)]PF_6$ (**13**[c])[27]	500	1.41	0.84	−1.10
$[Ru(tpy)(dpb\text{-}CO_2Me)]PF_6$ (**14**[c])[27]	492	1.38	0.89	−1.27

[a] Data collected using 0.1 M NBu_4BF_4 MeCN solutions at 100 mV/s and referenced to a $[Fc]/[Fc]^+$ internal standard followed by conversion to NHE ($[Fc]/[Fc]^+$ vs NHE = 0.64 V),[35] unless otherwise stated. [b] λ_{max} of lowest-energy band. [c] Potentials reported vs $[Fc]/[Fc]^+$ with NBu_4PF_6 as a supporting electrolyte, tabulated here vs NHE by adding +0.64 V. ttpy = 4′-toluyl-2,2′:6,2″-terpyridine; Hdpb-phenyl = 3,5-di(pyridin-2-yl)biphenyl; tpy-CO_2Et = 2,2′:6,2″-terpyridine-4′-carboxylic acid, ethyl ester; Hdpb-CO_2Me = methyl-3,5-di(pyridin-2-yl)benzoate.

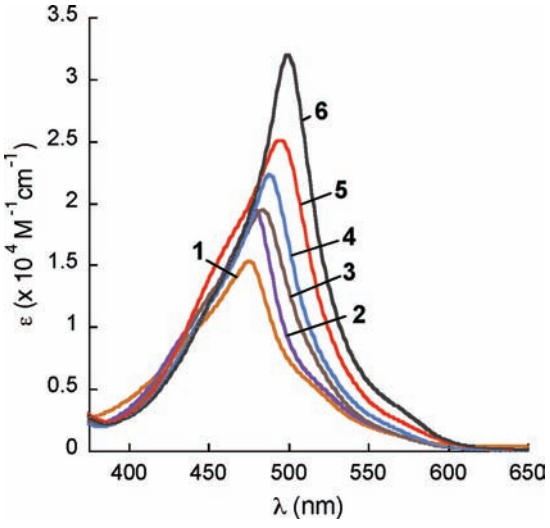

Figure 4. UV−vis spectra of compounds **1**−**6** in MeCN at ambient temperature.

metal d orbitals. The absorption profiles of **9** and **10** are similar, but the molar absorption for the latter is nearly 2-fold greater, which underscores the extent to which the −OMe substituent alters the light-harvesting properties of this molecule.

DFT Calculations. B3LYP/LanL2DZ DFT calculations were carried out on all compounds to aid in the determination of the electronic structure, while TD-DFT calculations on optimized geometries in MeCN were employed to model the corresponding absorption spectra for all compounds. The correlation of theory to the

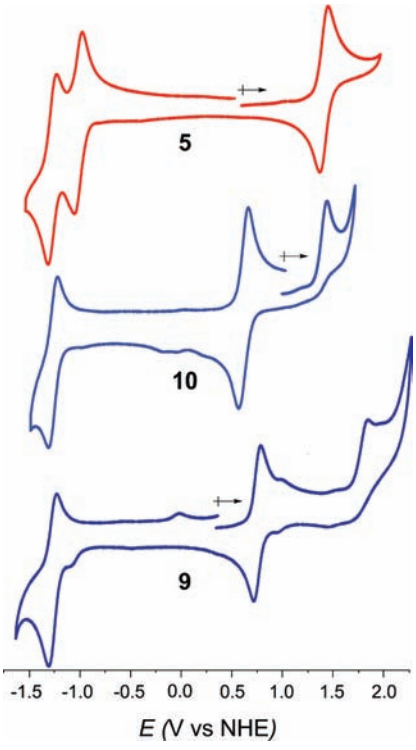

Figure 5. Cyclic voltammograms of complexes $[Ru(tpy\text{-}2\text{-}furyl)(tpy\text{-}OMe)](PF_6)_2$ (**5**, red), $[Ru(tpy\text{-}2\text{-}furyl)(dpb\text{-}OMe)]PF_6$ (**10**, blue), and $[Ru(tpy\text{-}2\text{-}furyl)(dpb)]PF_6$ (**9**, purple) in MeCN at ambient temperature (scan rate = 100 mV/s). Reversible redox potentials (vs NHE) are listed in Tables 1 and 2.

UV−vis spectra shown in Figure 6 is confined to transitions occurring over the 350−700 nm range. The experimental

data and the TD-DFT results show distinct differences between analogous non-cyclometalating and cyclometalating compounds (e.g., compounds **5** and **10**). As shown in the UV−vis absorption spectrum of **5** in Figure 6, the dominant feature in the visible region is a narrow MLCT absorption band centered at 495 nm (λ_1). TD-DFT calculations for **5** indicate that this transition arises primarily from the promotion of an electron from the d_{xz} metal orbital (HOMO) to the π^* orbital of the tpy-2-furyl ligand (LUMO).

Upon ligation of an analogous cyclometalating ligand (i.e., dpb-OMe instead of tpy-OMe), the UV−vis absorption changes in two distinct ways: (i) a red shift and broadening of the low-energy transitions occurs, and (ii) the appearance of a new higher-energy absorption band near 400 nm. We note that the electron density of the HOMO of the cyclometalated compounds contains significant ligand character on the central phenyl ring of the dpb-R^1 ligand.[27] Consequently, absorption bands over the 350−700 nm range represent transitions with mixed-metal−ligand-to-ligand and intraligand charge-transfer character. Because the latter makes a lower relative contribution to the spectra, these bands will be broadly defined as MLCT bands herein for brevity; however, a full listing of the transitions is provided in the Supporting Information. The absorption bands for **10** centered at 523 nm arise largely from two dominant MLCT transitions characterized as HOMO−1 → LUMO+1 (λ_4) and HOMO−2 → LUMO+1 (λ_3). These transitions correspond to the promotion of electrons from the d_{xz} and d_{xy} metal orbitals to the π^* system of the tpy-2-furyl ligand, respectively. The lower-energy shoulder at ~600 nm (λ_5) is ascribed to a MLCT process involving the promotion of an electron from the mixed metal−ligand HOMO to the LUMO derived from the π^* system of the tpy-2-furyl ligand. The high-energy transitions centered below 400 nm (λ_2) are due to MLCT transitions from the d_{yz} orbital to the high-energy π^* level of the cyclometalating dpb-OMe ligand.

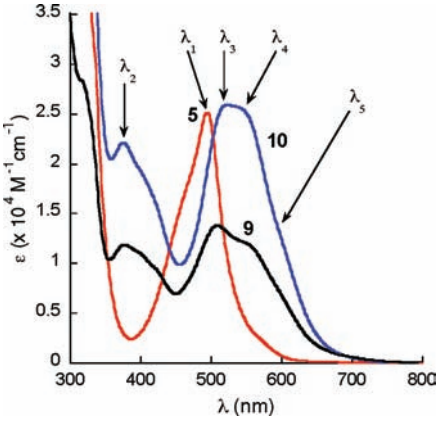

Figure 6. UV−vis spectra for complexes [Ru(tpy-2-furyl)(tpy-OMe)]-$(PF_6)_2$ (**5**, red), [Ru(tpy-2-furyl)(dpb-OMe)]PF_6 (**10**, blue), and [Ru(tpy-2-furyl)(dpb)]PF_6 (**9**, black) in MeCN at ambient temperature. Assignments for λ_n are provided in Figure 7.

Discussion

Our motivation for studying these series of Ru(II) complexes was to determine whether the electrochemical and photophysical properties could be adjusted appropriately for sensitizing semiconducting materials (e.g., TiO_2) in the context of solar energy conversion schemes (e.g., DSSC). To this end, a suite of compounds was selected to systematically elucidate how altering electronic dipoles across a series of polypyridyl and cyclometalated Ru complexes should affect the electronic properties. We advanced this study on the basis that substituted cyclometalating ligands complemented by derivatized π-accepting polypyridyl-based ligands would render a bathochromic shift in the absorption profile.

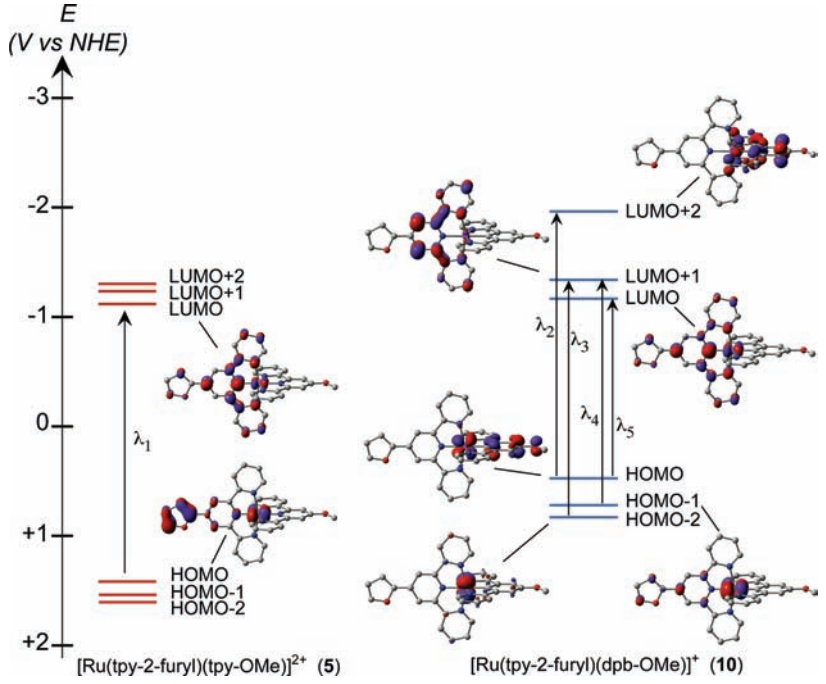

Figure 7. Energy-level diagram generated from the TD-DFT calculations for **5** and **10**. Prominent electronic transitions (λ_n) and select molecular orbitals are shown (see Figure 6 for correlation of the λ_n transitions to the experimental spectra).

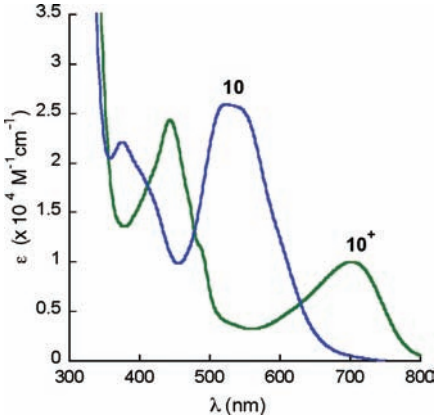

Figure 8. UV−vis spectra for complexes [Ru^{II}(tpy-2-furyl)(dpb-OMe)]PF_6 (**10**) and [Ru^{III}(tpy-2-furyl)(dpb-OMe)]$(PF_6)_2$ (**10**$^+$) in MeCN at ambient temperature.

Furthermore, we anticipated that heteroleptic complexes would introduce a higher number of electronic transitions, which would effectively broaden the absorption envelope. Electrochemical and spectroscopic properties in combination with TD-DFT studies provide a reasonably accurate description of the effects of structural and electronic dissymmetry.

This study also builds on the concept that the $Ru^{II/III}$ oxidation potential is significantly altered by the anionic cyclometalating ligand and that the electron-rich nature of this ligand results in a more polarizable complex. Considering the mixed metal−ligand character of the HOMO, there is a greater inherent sensitivity to electronic perturbation caused by substitution para to the organometallic bond. For instance, the addition of a −OMe group in the tpy series produces a mere 70−80 mV change; however, this same substituent results in a 130−140 mV difference within the cyclometalated series. Similar trends are observed for the absorption maxima: the −OMe group modestly perturbs the HOMO in the tpy series to induce a slight red-shift in the absorption spectrum, while this same substituent in the cyclometalated series increases the energy of the HOMO resulting in a larger bathochromic shift. These observations are consistent with the HOMO of the cyclometalated series having greater mixed metal−ligand character than that of the tpy series (Figure 7).[7,27] Delocalization of the HOMO over both the phenyl ring and the metal facilitates enhanced electronic communication between the π-donating −OMe substituent and the Ru center. The LUMO for both series remains relatively unaltered because electron density is localized primarily on the tpy ligand in both series.

The electron-rich cyclometalated complexes were found to be susceptible to oxidation, a consequence of the increased electron density on the metal center. Indeed, all of the dpb-OMe complexes readily oxidized in solution over a 15 min period. The UV−vis spectra in Figure 8 showcase the divergent spectral features of the diamagnetic **10** and paramagnetic oxidation product **10**$^+$. The high-energy transition of **10**$^+$ is assigned to a MLCT, while the lower-energy transitions emanate from a ligand-to-metal CT transition. Although this oxidation is suppressed upon the addition of ascorbic acid, complexes **8**, **9**, and **10** were inherently unstable in solution, thereby rendering chromatography and NMR measurements difficult.

Another drawback to the electron-rich cyclometalated complexes is an inherent instability toward oxidizing conditions, as shown by the irreversible oxidation wave in Figure 5. This feature explains the difficulty in generating [Ru(tpy-CO_2H)(dpb-R^1)]$^{1+}$ via the oxidation of the tpy-2-furyl precursors **9** and **10**. The low oxidation potentials and mixed metal−ligand character of the HOMO seems to provide a decomposition pathway which precludes the isolation of the carboxylic acid derivative. Although our synthetic approach failed to successfully yield electron deficient cyclometalating ligands, it has been previously shown[27] that cyclometalating ligands are also polarized using electron withdrawing groups.

Although the generation of the carboxylic acid derivative − our initial target − proved elusive, the analysis of the complexes containing the 2-furyl ring led to the serendipitous discovery that the 2-furyl substituent has a substantial positive effect on the extinction coefficient. While this could have been predicted by considering the extended conjugation, we contend that a more subtle feature is operative, namely, an electron-rich, low-resonance energy that results in a greater polarizability within the molecule akin to the effects seen in conjugated thiophenes,[40] pyrroles,[41] and porphyrins.[42,43] The 2-furyl ring appears to act as an electron donor in the tpy-based complexes, as evidenced by a decrease in the $Ru^{II/III}$ oxidation potential, but displays modest acceptor character within the cyclometalated series on the basis of the ^{1}H NMR data and metal-based oxidation potentials.

The aforementioned donor/acceptor gradient and polarizability of these molecules will not only benefit the light-harvesting efficiency of these complexes but we postulate that these features will enhance their electron-transfer kinetics within the DSSC. By directing the induced dipole toward the semiconducting material, the rate of electron injection into the anode should be enhanced. Furthermore, the delocalization of the HOMO over the non-anchored cyclometalated ligand will not only increase the optical cross-section of these dyes, it should also aid the regeneration of the oxidized dye by the electrolyte.

Conclusions

This study highlights the viability of using substituted cyclometalated compounds in light-harvesting applications.[1,4,7] Cyclometalation of the metal is shown to be an effective way to increase the electron density at the metal center, which raises the energy of the HOMO relative to the tpy congeners. The photophysical and electrochemical properties of these complexes can be further tuned using suitable electron-withdrawing and electron-donating groups at the 4′ position of the tpy or dpb^- ligands. In fact, the cyclometalated species are more sensitive than their tpy-based congeners to substitution at the site para to the Ru−C bond of the central ring. Indeed, judicious choice of substituents at the 4′ position leads to a significant red shift in the absorption profile coupled with an enhanced molar absorptivity. This approach imparts

(40) Jungermann, S.; Riegel, N.; Muller, D.; Meerholz, K.; Nuyken, O. *Macromolecules* **2006**, *39*, 8911–8919.
(41) Grabulosa, A.; Martineau, D.; Beley, M.; Gros, P. C.; Cazzanti, S.; Caramori, S.; Bignozzi, C. A. *Dalton Trans.* **2009**, 63–70.
(42) Campbell, W. M.; Burrell, A. K.; Officer, D. L.; Jolley, K. W. *Coord. Chem. Rev.* **2004**, *248*, 1363–1379.
(43) Kay, A.; Grätzel, M. *J. Phys. Chem.* **1993**, *97*, 6272–6277.

greater electron density and polarizability within the molecule to enhance the light-harvesting properties over a greater fraction of the solar spectrum.

Acknowledgment. This work was financially supported by the Canadian Natural Science and Engineering Research Council (NSERC), Canada Research Chairs, Canadian Foundation for Innovation, Alberta Ingenuity, Canada School for Sustainable Energy, and the Institute for Sustainable Energy, Environment & Economy.

Supporting Information Available: Calculated UV−vis spectra for compounds **1**−**10**. This material is available free of charge via the Internet at http://pubs.acs.org.